CELLULAR NEUROSCIENCE

Septal GABAergic inputs to CA1 govern contextual memory retrieval

Arnau Sans-Dublanc[1]*†, Adrià Razzauti[1†‡], Srinidhi Desikan[2], Marta Pascual[3,4], Hannah Monyer[2], Carlos Sindreu[1§‖]

The CA1 output region of the hippocampus plays an essential role in the retrieval of episodic memories. γ-Aminobutyric acid–releasing (GABAergic) long-range projections from the medial septum (MS) densely innervate the hippocampus, but whether septal inputs regulate memory expression remains elusive. We found that the MS to CA1 connection is recruited during recall of a contextual fear memory. Chemogenetic silencing of CA1-projecting MS neurons or septal GABAergic terminals within CA1 blocked memory retrieval. Photostimulation of septal GABAergic terminals in CA1 selectively inhibited interneurons. Abrogating septal GABAergic cells during retrieval disinhibited parvalbumin-rich (PV+) cells in CA1. Direct activation of CA1 PV+ cells impaired memory and prevented the induction of extracellular signal–regulated kinase/mitogen-activated kinase signaling in postsynaptic pyramidal neurons. Opposing disinhibition of hippocampal PV+ cells reversibly restored memory. Our data indicate that suppression of feed-forward inhibition onto CA1 by septal GABAergic neurons is an important mechanism in gating contextual fear behavior.

INTRODUCTION

Memory retrieval, or the access to stored information in the brain, guides several adaptive behaviors (*1*), and its precision or success is likely to be impaired during dementia or autism (*2*, *3*). Although the distributed networks supporting retrieval are not well understood, experimental studies point to the CA1 output region of the hippocampus as a critical node for the recall of episodic memory, such as contextual conditioning (*4*–*6*). In this paradigm, memory retrieval is reliably inferred from the rapid freezing behavior (i.e., a rodent's natural response to threat) upon reexposure to the conditioning box, triggering context-specific signatures at the cell firing (*7*) or molecular levels (*8*). Considerable progress has linked CA1 pyramidal cell activation with afferences in CA3 or entorhinal cortex (*9*–*11*) and with downstream circuits in the subiculum (*12*) or neocortex (*13*) during contextual recall. However, the hippocampus also receives long-range γ-aminobutyric acid–releasing (GABAergic) projections from the subcortical medial septum (MS)/diagonal band that terminate on interneurons (*14*, *15*), convey sensory stimuli (*16*), and degrade with aging (*17*). MS^{GABA} inputs disinhibit hippocampal pyramidal cells (*18*) and contribute to rhythmic oscillations necessary during rapid eye movement sleep for memory consolidation (*19*). Despite these advances, very little is known about the role of ascending MS projections in retrieval in animal models or in human cognition in general (*20*). In rodents, the MS promotes theta oscillations in the local field potential that are associated with higher cortical input and dendritic depolarization at the peak and with higher CA3 input and somatic spiking at the trough. On this basis, it was postulated that theta helps partition new and stored information by allowing them to be most active at different times within the theta cycle when encoding or retrieval do occur (*21*). An untested prediction from this model is that MS interventions should also regulate retrieval. Moreover, the cell types and molecular cascades mediating the presumed effect of MS on memory retrieval have not been investigated. Here, we addressed the hypothesis that inhibitory control of CA1 interneurons by septal GABAergic inputs promotes retrieval of contextual memory and associated neural signal transduction.

RESULTS

Septal input to CA1 is activated during memory retrieval

To examine the function of the MS-CA1 pathway in memory retrieval, we first injected into the dorsal CA1 region a herpes simplex virus expressing yellow fluorescent protein (HSV-YFP) for high-efficiency brain-wide retrograde cell tagging (fig. S1, A to C). Up to 7 ± 1% of CA1-projecting cells originated from the MS (Fig. 1A). MS^{CA1} cells were predominantly GABAergic (~86%), and, in dorsal and medial divisions, they concentrated within ~200 μm from midline, where the ratio of GABAergic to cholinergic cells was highest (fig. S1, D to F). In control studies with two additional retrograde vectors, retrograde adeno-associated vector (AAV2-retro) and CAV2 (canine adenovirus type 2), we found a similar fraction of GABAergic MS^{CA1} cells (fig. S1, G to I). To selectively label MS-CA1 projections, we combined CA1 injection with CAV2 expressing Cre recombinase, followed by injection into the MS of AAV-Flex-tdTomato for conditional expression of red fluorescent protein (RFP) (Fig. 1B). Axons of MS^{CA1} cells mainly targeted the CA1, dorsal subiculum, or lateral perforant path, indicating little collateralization (fig. S2, A and B). Consistently, colabeling of MS cells projecting to the entorhinal cortex (EC), another known target, revealed intermingled but segregated subpopulations (fig. S2, C and D). To test whether the MS-CA1 pathway is recruited during memory retrieval, we trained mice for contextual fear conditioning and quantified the presence of c-Fos, a

[1]Pharmacology Unit, Department of Clinical Foundations, University of Barcelona, Barcelona 08036, Spain. [2]Department of Clinical Neurobiology of University Hospital and DKFZ, Heidelberg, Germany. [3]Department of Cell Biology, Physiology and Immunology, University of Barcelona, Barcelona 08028, Spain. [4]Centro de Investigación Biomédica en Red sobre Enfermedades Neurodegenerativas (ISCIII), Madrid, Spain.
*Present address: Department of Biology, Neuro-Electronics Research Flanders, KU Leuven, Belgium.
†Co-primary authors.
‡Present address: Laboratory of Neurophysiology, ULB Neuroscience Institute, Brussels, Belgium.
§Present address: Institut d'Investigacions Biomèdiques August Pi i Sunyer, Barcelona 08036, Spain.
‖Corresponding author. Email: csindreu@ub.edu

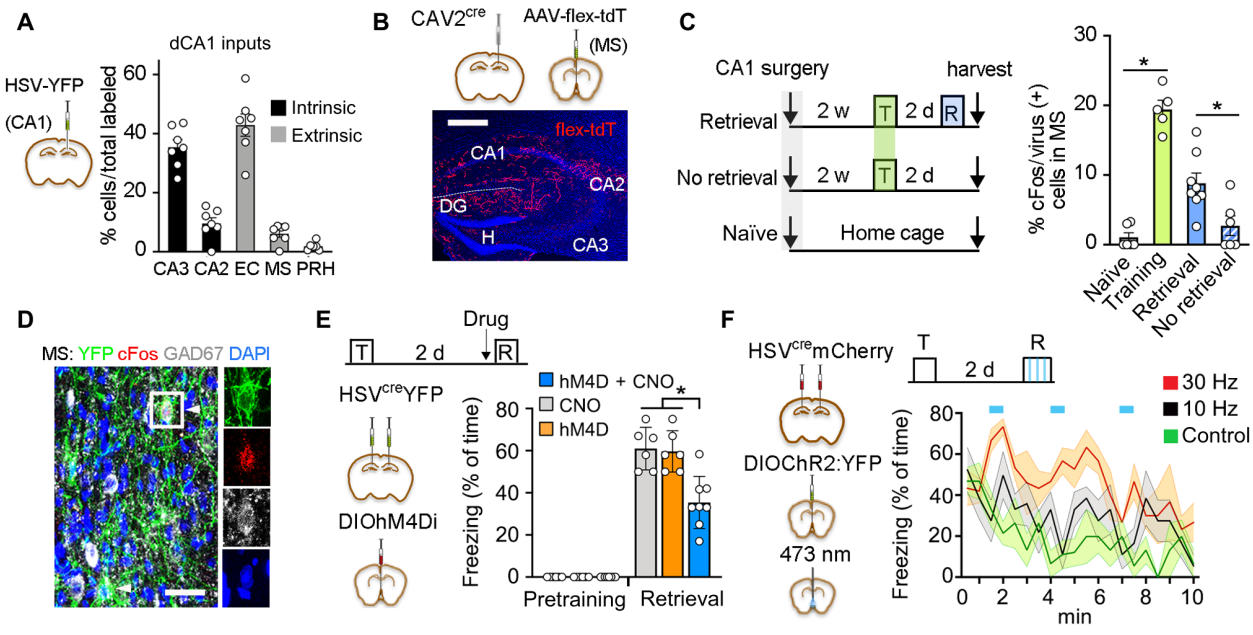

Fig. 1. CA1-projecting MS neurons support retrieval of contextual fear memory. (**A**) Delivery of HSV-YFP into the CA1 labels afferent cells in other hippocampal subfields (intrinsic) or brain regions (extrinsic) ($n = 7$ mice). (**B**) Labeled axons from MS^{CA1} cells. Scale bar, 0.5 mm. (**C**) cFos expression in MS^{CA1} cells from naïve ($n = 6$), trained (T; $n = 5$), reexposed (R/retrieval; $n = 8$), or not reexposed (no retrieval; $n = 6$) mice. Training or retrieval increased cFos immunoreactivity [$F_{(3,25)} = 36.6$, $P < 0.0001$; post hoc tests, training versus naïve, $P < 0.0001$; retrieval versus naïve, $P = 0.0009$; retrieval versus no retrieval, $P = 0.012$]. (**D**) Colabeling of HSV-derived YFP, cFos, and GAD in MS after retrieval. Scale bar, 0.02 mm. (**E**) Inhibition of MS^{CA1} neurons during retrieval test [effect of treatment, $F_{(2,34)} = 12.3$, $P < 0.0001$; effect of conditioning, $F_{(1,34)} = 438$, $P < 0.0001$; interaction, $F_{(2,34)} = 12.3$, $P < 0.0001$; inhibited versus controls, $P < 0.0001$]. (**F**) Photostimulation of MS^{CA1} during retrieval [YFP, $n = 6$ mice; ChR2:YFP, 10 Hz, $n = 6$ mice; ChR2:YFP, 30 Hz, $n = 4$ mice; effect of stimulation, $F_{(2,13)} = 18.52$, $P = 0.0002$; effect of time, $F_{(2,13)} = 3.71$, $P = 0.0016$]. Shaded colors indicate SD.

marker of recent activation, in retrogradely tagged cells. Both conditioning and contextual reexposure, which evoked marked freezing behavior (fig. S3, A and B), induced a significant increase in c-Fos expression compared with controls (Fig. 1, C and D).

The GABAergic septal to CA1 connection supports contextual memory

We expressed the inhibitor receptor hM4Di fused to mCherry in MS^{CA1} cells using a conditional approach as above (fig. S3C). Targeted neurons were then inhibited with injection of the agonist CNO (clozapine-N-oxide) before the retrieval test. Selective inhibition of MS^{CA1} neurons impaired fear memory compared with mice injected with vehicle or mice expressing YFP and receiving CNO (Fig. 1E). Conversely, MS^{CA1} neurons were transduced with channelrhodopsin (AAV-DIOChR2:EYFP) and their cell bodies photostimulated at 10 or 30 Hz [i.e., their natural frequency range (*19*)] in 30-s epochs during contextual reexposure. Although all groups showed a gradual decline in freezing over the course of 10 min, light pulses transiently increased it in a frequency-dependent manner compared with YFP control (Fig. 1F). Similar treatment in a neutral context failed to evoke freezing or alter locomotion (fig. S3, D to G).

The above results indicate that MS^{CA1} neurons are critical for memory recall and suggest that GABAergic septal (MS^{GABA}) terminals in CA1 can support such function. To directly test this hypothesis, we injected GAD (glutamic acid decarboxylase)–cre mice with AAV-FlexPSAM^{L141F}:GlyR to express the Cl-permeable, chimeric receptor exclusively in MS^{GABA} neurons, followed by bilateral cannulae in CA1 for local injection of its agonist PSEM (pharmacologically selective effector molecule) (Fig. 2A). PSAM (pharmacologically selective actuator molecule):Gly identified with α-bungarotoxin was highly expressed at distal septo-hippocampal terminals (Fig. 2B). PSEM infusion confined to CA1 (fig. S4, A and B) impaired memory retrieval compared with controls (Fig. 2C), supporting the conclusion that the MS^{GABA}-CA1 pathway is required for contextual recall.

Separate GAD-cre mice conditionally expressing hM4Di:mCherry in MS^{GABA} cells also showed a deficit in contextual memory upon systemic CNO injection before retrieval test (Fig. 2D and fig. S4D). In contrast, tone-evoked memory, which does not rely on the hippocampus (*22*), was spared by MS^{GABA} inhibition, and it failed to induce c-Fos in MS^{CA1} cells (fig. S4, E to G and I). Open field behavior was also spared (fig. S4H), together ruling out indirect effects of MS^{GABA} or a deficit in expressing a normally retrieved memory.

Reactivation of the extracellular signal–regulated kinase (Erk)/mitogen-activated protein kinase (MAPK) signaling cascade is one of the few established molecular correlates of memory expression, particularly in the CA1 region (*8*, *23*). Levels of the active, dually phosphorylated form of Erk1/2 (i.e., pErk) increased following memory retrieval in CA1, but not in other brain regions targeted by MS^{GABA} axons (fig. S5). Notably, the induction of pErk in CA1 pyramidal cells [i.e., WFS1+ (Wolfram syndrome protein)] was strongly suppressed when MS^{CA1} neurons, MS^{GABA} terminals in CA1, or MS^{GABA} cells were specifically inhibited compared with controls (Fig. 2, E and F), demonstrating that the MS^{GABA}-CA1 pathway is instrumental for memory-associated MAPK activation.

CA1 interneurons mediate the effect of septal GABAergic inputs on retrieval

To elucidate the microcircuit involved, we obtained acute hippocampal slices from GAD-cre mice previously injected in the MS with AAV-DIOChR2:mCherry (fig. S6, A and B). Under voltage

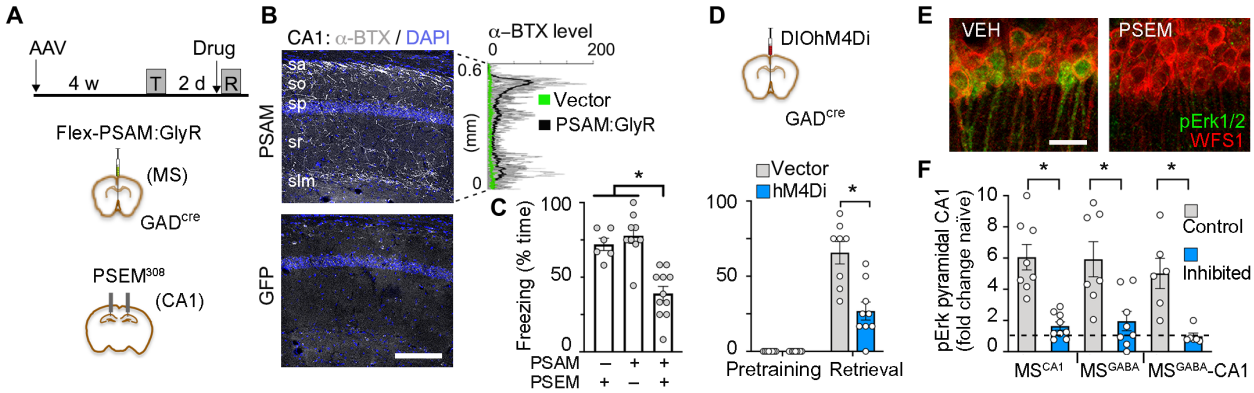

Fig. 2. Septo-hippocampal GABAergic inputs in recall and associated Erk1/2 activation. (**A**) Experimental design. (**B**) Bungarotoxin fluorescence (α-BTX) and line scans in grayscale across CA1 layers [PSAM versus green fluorescent protein (GFP), unpaired *t* test, $P = 0.01$]. sa, stratum alveus; so, oriens; sp, piramidale; sr, radiatum; slm, lacunosum-moleculare. (**C**) Inhibition of MS^{GABA}-CA1 inputs at retrieval test [PSAM + PSEM, $n = 11$; PSAM + vehicle (VEH), $n = 9$; GFP + PSEM, $n = 6$; effect of treatment, $F_{(2,26)} = 22.4$, $P < 0.0001$; PSEM versus VEH, $P < 0.0001$; GFP versus PSAM, $P = 0.0005$; GFP versus VEH, $P = 0.738$]. (**D**) Inhibition of MS^{GABA} cells at retrieval test [vector, $n = 8$; hM4D, $n = 9$; effect of treatment, $F_{(2,15)} = 16.6$, $P = 0.001$; effect of conditioning, $F_{(1,15)} = 94.8$, $P < 0.0001$; interaction $F_{(2,15)} = 16.6$, $P = 0.001$; vector versus hM4D at retrieval, $P < 0.0001$]. (**E**) pErk labeling in CA1 pyramidal cells after VEH or PSEM infusion during retrieval in mice expressing PSAM as in (A). (**F**) pErk level 15 min after retrieval test in the three treatment groups [effect of treatment, $F_{(5,44)} = 10.1$, $P < 0.0001$; control versus inhibited comparisons, MS^{CA1} cells, $P = 0.0006$; MS^{GABA} cells, $P = 0.0047$; MS^{GABA}-CA1 terminals, $P = 0.0123$].

clamp, light pulses elicited synaptic currents that were blocked by tetrodotoxin (TTX) and revived after the addition of 4-AP, suggesting a monosynaptic connection (Fig. 3A). The response persisted in the presence of CNQX/D-AP5, and it was only blocked after the addition of gabazine, thereby confirming septal GABAergic input. All (13 of 13) fast-spiking (FS) cells and 83% (34 of 41) of non-FS cells showed suppressed firing during optogenetic stimulation (Fig. 3B and fig. S6, C and D). In contrast, 6% (3 of 47) of pyramidal cells and none of the giant radiatum cells (0 of 3) responded to stimulation. We also injected GAD-cre mice in the MS with an anterograde trans-synaptic virus, AAV1-DIOFlpo (*24*), followed by injection in CA1 of AAV5-fDIO-YFP for genetic amplification. Somata expressing Flp recombinase and, hence, Flp-dependent YFP mainly lied in the pyramidal cell layer and expressed interneuron markers in various proportions (fig. S6, E to H); a large subset was parvalbumin rich (PV+). MS^{GABA} inputs may therefore limit the recruitment of inhibition during successful recall. Consistent with this notion, acute suppression of MS^{GABA} gated the activation of FS/PV+ cells in CA1 ($CA1^{PV}$), alongside with memory deficits (Fig. 3C). In contrast, non-PV, GAD67+ interneurons in CA1 or PV+ cells in DG were spared in the same animals (fig. S7).

Because the role of $CA1^{PV}$ cells on memory retrieval is unclear, we conditionally expressed the excitatory receptor hM3Dq:mCherry in dorsal CA1 of PV-cre mice (fig. S8, A to C), i.e., mainly in basket and bistratified inhibitory cells (*25*). Mice froze significantly less in response to CNO during contextual reexposure compared with vehicle (Fig. 3D); they also showed a strong deficit in pErk1/2 in pyramidal cells that was inversely correlated with $CA1^{PV}$ cell activation (Fig. 3E and fig. S8, D to H). Arguing against nonspecific deficits, the same PV-cre mice showed modest improvement in a Y-maze spatial working memory task when treated with CNO in a permutated design study performed 1 week before conditioning (fig. S8I).

Whether pan-neuronal inhibition of MS would also impair retrieval is unclear. Moreover, if the effects of MS and $CA1^{PV}$ on memory were functionally related, then opposing disinhibition of the latter should improve memory retrieval. Thus, we expressed SynI-hM4D in MS cells, and the conditional inhibitory receptor KORD (κ-opioid-derived designer receptor) in $CA1^{PV}$ cells of PV-cre mice (Fig. 3F); the use of unique ligand/receptor pairs allowed for independent control of each population. Here, we activated hM4D with C21 instead of CNO given its superior brain permeability (*26*). Conditioned mice were tested for memory on three consecutive days. As with MS^{GABA} or MS^{CA1}, MS inhibition (i.e., C21 injection during retrieval test) impaired memory compared with vehicle (Fig. 3G). Amnesia was prevented by concomitant inhibition of $CA1^{PV}$ cells on the second day (i.e., salB + C21 coinjection), whereas salB injection alone did not differ from vehicle. The memory deficit reemerged when MS was again blocked alone on the third day. No effect of day was found in vehicle-injected mice. The reversibility of the amnesia suggests the memory trace was preserved during MS block. Freezing scores were mirrored by changes in ambulatory distance and resting time (Fig. 3H). Together, the results point to PV+ cells as necessary for the effect of the MS-CA1 pathway on contextual memory recall.

DISCUSSION

We provide direct evidence that expression of contextual fear behavior is causally related to activation of a septal GABAergic projection to the CA1 hippocampus, restricting local inhibitory control to enable activation of MAPK signaling in memory-holding pyramidal cells (fig. S9) (*4*, *6*, *8*, *21*). The predominance of glutamic acid decarboxylase among the CA1-projecting septal neurons after retrograde labeling with different vectors, and the largely restricted role of cholinergic signaling to the encoding phase of memory (*27*), suggested that a GABAergic mechanism supported retrieval. This was confirmed by selectively manipulating the septal GABAergic component in GAD-cre mice, which showed a similar phenotype as with pan-neuronal MS inhibition. Factors contributing to the abundance of GABAergic neurons among MS^{CA1} cells may include the greater GABAergic-to-cholinergic cell ratio in central parts of the MS, the larger size of GABAergic terminals for viral uptake, or a subregional specification of septal inputs.

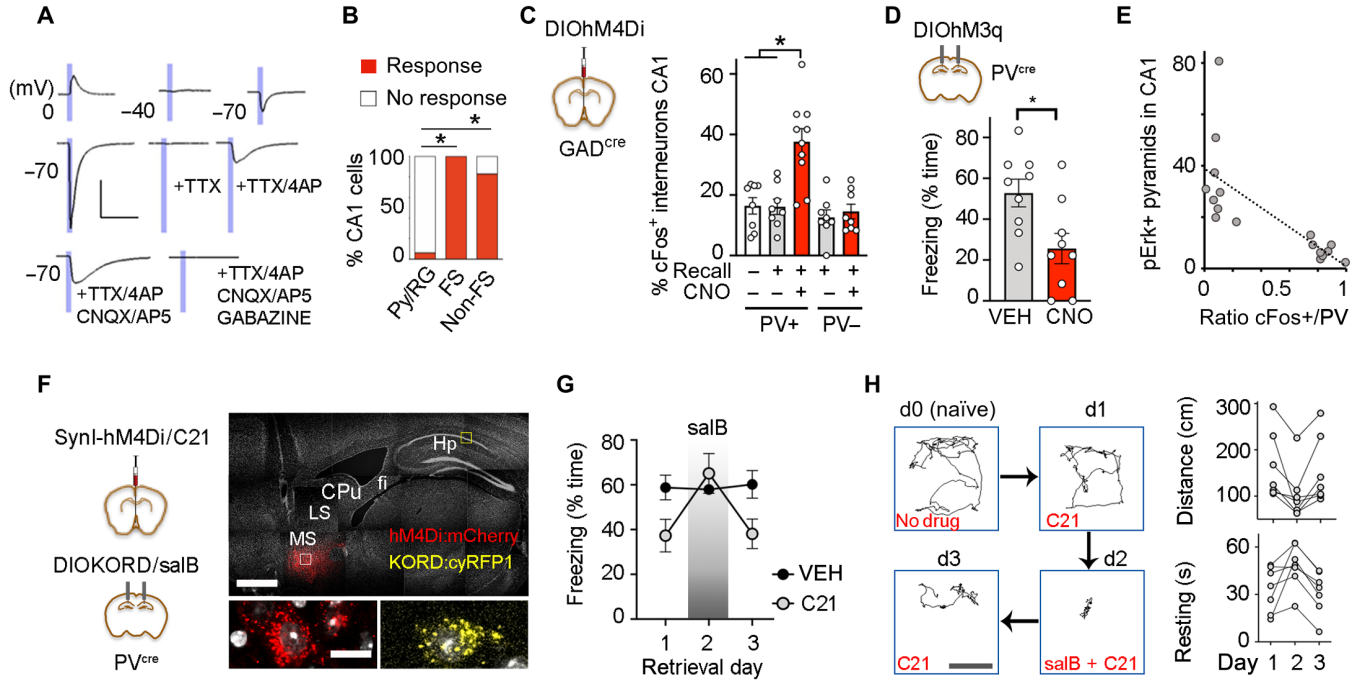

Fig. 3. Feed-forward interneurons mediate the effect of MS^{GABA} on memory retrieval. (**A**) Response traces upon photostimulation of septal axons in CA1 at different voltages and during consecutive drug applications. Scale, 200 pA and 40 ms. (**B**) Responding cells upon photostimulation of MS^{GABA} fibers (Fisher's exact test, excitatory versus FS, $P < 10^{-10}$; excitatory versus non-FS, $P < 10^{-13}$). (**C**) Effect of MS^{GABA} inhibition on c-Fos [$F_{(4,37)} = 12.7$, $P < 0.0001$; only recall in CNO for CA1 PV+ cells differed from naïve, $P = 0.01$, or vehicle, $P = 0.007$]. (**D**) hM3q stimulation of CA1^{PV} cells during retrieval (unpaired t test, $t = 2.7$, $P = 0.015$; $n = 9$ per group). (**E**) Inverse cell correlation following retrieval ($r = -0.72$, $t = -3.72$, $P = 0.002$). (**F**) Expression of hM4Di in MS and KORD in CA1 in a sagittal slice, 30° angle. Scale bars, 1 mm (top) and 10 μm (bottom). LS, lateral septum; CPu, caudate putamen; fi, fimbria; Hp, hippocampus. (**G**) Freezing at retrieval test [daily vehicle, $n = 6$; daily C21, $n = 7$; day × treatment interaction $F_{(2,22)} = 6.95$, $P = 0.0046$; freezing in VEH versus VEH + salB, $P = 0.98$; C21 versus C21 + salB, $P = 0.0006$]. (**H**) Left, daily trajectories from a subject during the first 110 s. Right, distance and immobility in C21-treated mice (C21 versus C21 + salB for distance, $P = 0.031$, and for resting time, $P < 0.0001$).

Our results help to dissociate the innate effect of MS on locomotion, likely supported by glutamatergic inputs (*28*), from that on freezing behavior. Silencing septal GABAergic cells spared several parameters in the open field, but it consistently impaired fear memory retrieval. By encoding the intensity of multisensory cues (*16*), septo-hippocampal GABAergic boutons may calibrate behavioral or autonomic responses (*12*) upon contextual reexposure. Further, the enhanced response of MS^{CA1} cells to conditioned stimuli following learning parallels observations in the parabrachial nucleus (*29*) and suggests a mechanism underlying the efficiency of memory recall. The preferential disinhibition of PV+ cells in CA1 following MS^{GABA} blockade is consistent with our circuit tracing results and with the greater density of excitatory synapses described onto PV+ cells compared with other interneurons (*30*). Crucially, opposing such disinhibition restored memory, functionally linking the effects of MS and CA1^{PV} cells on memory recall. Our results support computational models predicting that septal GABAergic inhibition can facilitate memory retrieval by occluding feed-forward interneurons (*31*), a process that may increase transfer of stored information to CA1. The ability of the MS^{GABA}-CA1 pathway to prevent the induction of PV+ cell activation is also analogous to the disinhibition of excitatory outputs in the prefrontal cortex that gates fear expression (*32*).

Similar circuit motifs involving long-range GABAergic inputs from the entorhinal cortex (*33*) or brainstem (*34*) have been shown to modulate learning. These mechanisms spared PV+ hippocampal interneurons and mainly targeted plasticity at distal dendrites. One possible merit of such organization may be to reduce interference between encoding and recall of episodic memory.

We found that MS^{CA1} cells were largely segregated from the septal projection to caudal EC. The MS facilitates grid-like activity in EC, where stellate cells support memory recall and contextual representations downstream in CA3 (*10*). Thus, the MS-EC pathway might also feed salient information to the hippocampus and, in coordination with MS^{CA1} inputs, allow for sensory-evoked recall. Moreover, since recruitment of the EC is thought to increase at remote time points (*35*), it may be worth exploring in the future whether MS-EC projections have a greater influence on recall following systems consolidation.

We identified MS^{CA1} cells as a site of plasticity that promotes memory recall, but the specific synaptic modifications that may also be involved remain unclear. Previous work failed to observe changes in inhibitory inputs to CA1^{PV} cells after fear conditioning (*36*). Alternatively, intrinsic excitability or brainstem inputs arriving to the MS might be strengthened (*16*), facilitating septal reactivation during retrieval. MS^{CA1} cells were also activated during conditioning, a time when the aversive stimulus may recruit the cholinergic component to shape the specificity of learning (*37*). The use of engram labeling technology may help establish whether such MS^{CA1} inputs are also required for memory consolidation, as suggested (*19*), or whether they enhance reactivation of CA1 pyramidal cells that were active during conditioning to promote memory recall.

The MS^{GABA}-CA1 projection is qualitatively different from the excitatory septal outputs that encode innate valence (*38*), but together

highlight the capacity of the MS to orchestrate learned and innate emotional responses through anatomically segregated pathways.

The role of the human MS (i.e., septum verum) in memory remains understudied (*20*). Despite intrinsic limitations of species differences, our results identified a targetable cellular circuit for developing novel therapeutic interventions to treat memory deficits in human patients.

MATERIALS AND METHODS

Animals

Procedures involving mice were performed in accordance with EU guidelines (2010/63/EU) and had ethical approval from the animal and ethical committee at University of Barcelona and from the Regierungspräsidium Karlsruhe, Germany (G-254-14). Adult C57BL/6J mice were supplied by Charles River Laboratories. GAD2-Cre and PV-cre mice of either sex and expressing Cre recombinase in glutamic acid decarboxylase or PV-positive cells were bred in-house on a C57BL6 background and used at 2 to 5 months of age. Mice had unrestricted access to water and food and maintained on a 12-hour light cycle.

Viral constructs

Herpes viruses (HSV-EF1a-YFP and HSV-cre-EF1a-YFP/mCherry) were supplied by the Massachusetts Institute of Technology Viral Gene Transfer Core at titers of 3.5×10^8 IU/ml. CAV2-cre virus was provided by M. Chillon and amplified in-house to ~10^{12} viral genomes (vg)/ml. Adeno-associated vectors AAV8-EF1a-DIO-hM4Di-mCherry, AAV5-EF1a-DIO-hChR2(H134R)-EYFP, AAV5-EF1a-DIO-EYFP, and AAV1-CAG-flex-tdTomato were supplied by the University of North Carolina at Chapel Hill Vector Core facility at titers of 4×10^{12} to 7×10^{12} vg/ml. AAV1/2-hSyn-flex-PSAM^{L141F}:GlyR-IRES-GFP (Addgene plasmid no. 32479) was produced in-house by calcium phosphate–mediated transfection of 293T cells, purified by sucrose and CsCl gradient centrifugation steps, and resuspended in Hepes-buffered saline to ~10^{12} vg/ml. AAV1/2-DIO-hChR2(H134R)-mCherry was obtained from K. Deisseroth. AAV5-hSyn-DIO-hM3Dq-mCherry was supplied by Addgene (#44361) at 7×10^{12} vg/ml. AAV1-EF1a-DIO-FLPo (Addgene plasmid no. 87306) was produced by Vigene Biosciences at 2×10^{13} vg/ml. AAV5-CAG-dFRT-EYFP at 1×10^{13} vg/ml, AAV8-SynI-hM4D-mCherry at 7×10^{12} vg/ml, AAV/retro2-synI-mCherry-2A-iCre at 4×10^{12} vg/ml, and AAV1/2-Dlx-DIO-KORD-mCyRFP1 at 4×10^{12} vg/ml were supplied by the viral vector facility at the Neuroscience Center Zurich.

Stereotaxic surgery

Mice were anesthetized with ketamine/xylazine and placed in a small-animal stereotaxic instrument [WPI (World Precision Instrument)]. Eyes were lubricated with ophthalmic ointment, fur shaved, skin sterilized, and bupivacaine locally administered at incision site. A small craniotomy was followed by viral injection or Alexa Fluor 488–conjugated cholera toxin B with a Hamilton syringe (33 gauge) at a rate of 35 nl/min for a total of 300 to 800 nl. Injection coordinates are given in millimeter, relative to bregma and brain surface, for dorsal CA1: −1.9 anteroposterior (AP), 1.4 mediolateral (ML), and −1.45 dorsoventral (DV); for MS: +1 AP, 0 ML, and −4 DV; for EC: −4.65 AP, 3.25 ML, and −2.8 DV. Recovery times before behavior were optimized for each virus: 2 weeks for HSV, 4 to 5 weeks for AAV-PSAM, 6 weeks for CAV2, and 3 to 4 weeks for other AAVs. For intra-hippocampal drug infusion or septal photostimulation, custom-made cannulae (30 gauge; Plastics1, Inc.) or fiber optic cannulae (200-μm diameter; Doric Lenses) were implanted after virus injection in the same surgery and secured with dental acrylic and microscrews.

Electrophysiology

GAD-cre mice were stereotaxically injected with 300 nl of AAV1/2-DIO-hChR2(H134R)-mCherry via a glass micropipette (tip resistance of 2 to 4 megohms). The scalp incision was sutured, and the mice were constantly monitored for proper recovery. Two weeks after surgery, mice were deeply anaesthetized with inhaled isoflurane, followed by transcardial perfusion with ~20 ml of ice-cold sucrose solution containing 212 mM sucrose, 26 mM $NaHCO_3$, 1.25 mM NaH_2PO_4, 3 mM KCl, 7 mM $MgCl_2$, 10 mM glucose, and 0.2 mM $CaCl_2$, oxygenated with carbogen gas (95% O_2/5% CO_2, pH 7.4). The 300-μm sections were cut in ice-cold oxygenated sucrose solution, followed by incubation in oxygenated extracellular solution containing 12.5 mM NaCl, 2.5 mM $NaHCO_3$, 0.125 mM NaH_2PO_4, 0.25 mM KCl, 2 mM $CaCl_2$, 1 mM $MgCl_2$, and 25 mM glucose. Individual slices were placed in a submerged recording chamber mounted on an upright microscope (Olympus BW-X51) and continuously perfused with oxygenated extracellular solution. Cells in CA1 of the hippocampus and in the MS were visualized with differential interference contrast optics, and epifluorescence was used to detect mCherry fluorescence.

We recorded from acute horizontal slices. The septal injection site was controlled in coronal sections. Recording pipettes were pulled from borosilicate capillaries with the tip resistance of 4 to 6 megohms and filled with an intracellular solution containing 105 mM K-gluconate, 30 mM KCl, 10 mM Hepes, 10 mM phosphocreatine, 4 mM Mg–adenosine 5′-triphosphate, and 0.3 mM guanosine 5′-triphosphate with pH adjusted to 7.3 with KOH. This intracellular solution causes the reversal potential of the chloride ions passing through the GABA channel to shift to −40 mV, thereby allowing GABAergic inputs to be observed better. Liquid junction potentials were not corrected for. Target cells in different layers of CA1 were patched and classified on the basis of firing patterns in current clamp mode by applying 1-s current pulses starting at −200 pA in 20-pA steps. To analyze the postsynaptic responses, cells were voltage clamped at −70 mV and were stimulated with 5-ms light-emitting diode stimulation at 470 nm. Bath-applied drug concentrations were: CNQX (10 μM), D-AP5 (50 μM), gabazine (10 μM), TTX (1 μM), and 4-AP (100 μM). All recordings were made using a HEKA PatchMaster EPC 10 amplifier, and signals were filtered at 3 kHz and sampled at 20 kHz. Data were analyzed offline with MatLab, and results are presented as mean ± SEM.

Fear conditioning

For context-evoked memory, mice were placed in a standard fear conditioning box (Coulbourn Instruments) wipe cleaned with 1% acetic acid, 40-dB white noise, and indirect room light. Following 2 min of exploration, they received a single 2-s 0.7-mA foot shock and removed 58 s later. One or 2 days later, they were placed back into the same context for 3 min to assess freezing. Naïve mice were never shocked. Behavior was automatically recorded with Smart software (Panlab), and freezing was hand scored every 5 s by blinded experimenters. For delayed tone conditioning, three 2-s 0.3-mA shocks were coterminated with 15-s 2-kHz, 80-dB tones delivered in succession at 60- to 90-s intervals. On day later, mice were placed in a different context (with bedding, round corners, and opaque walls cleaned with 10% ethanol) that evoked no freezing behavior

until the same 15-s tone was delivered four times at 1-min intervals. Freezing was scored every 2 s during each tone and the following 15 s.

For laser stimulation, mice had been acclimated for 3 days to fiber optic cables. During photostimulation experiments, light pulse trains (10-ms pulses at 10 or 30 Hz for 30 s) were programmed with a waveform generator (Agilent Technologies, model 33500B) that provided input to a blue light DPSS (diode-pumped solid state) laser (473 nm; LaserGlow). Light power exiting the fiber-optic cable was ~15 mW under continuous mode. Light trains were delivered three times at 2-min intervals during the retrieval test.

Open field

Mice were placed in an arena (40 cm by 40 cm by 40 cm) and allowed to explore for 5 min while behavior was recorded with Smart software. Center zone (25% area) was predefined. Move transitions were defined as movement events following a >2-s resting time (i.e., <0.5 cm/s). For photostimulation at 10 Hz, mice received three consecutive 30-s-long trains with 30-s intervals without light for a total of 5 min. For dose responses, stimulation at 7, 20, or 30 Hz was repeated four times at each frequency, the order being pseudorandomized for each animal. Speed at the periphery (i.e., excluding 25% center area) was video recorded at 30 frames/s during a 15-min session.

Y-maze

A discrete alternation version was used. Every trial consisted of two runs, and trials were repeated six times at 20-min intervals. In the first run of a given trial, the mouse was placed in the holding compartment that was connected through a sliding door to the start arm of a Y-maze (10 cm by 24 cm by 8 cm arms). The mouse was allowed to choose one of the two distal target arms, after which it was enclosed for 30 s. It was then returned to the holding chamber, and 5 s later allowed to run the maze again to record the target arm chosen (i.e., the same arm or the new, alternative arm).

Pharmacological injections

CNO (Enzo Biosciences) and C21 (Merck) were prepared in sterile 0.9% saline and 0.5% dimethyl sulfoxide (DMSO) and injected intraperitoneally 30 min before testing at 3 mg/kg; Salvinorin-B (Merck) was prepared in 100% DMSO and injected subcutaneously 15 min before testing at 10 mg/kg; PSEM-308 was prepared at 100× concentration in nuclease-free water and diluted to 100 µM in artificial cerebrospinal fluid the day of use. Intra-hippocampal infusion of PSEM or vehicle was performed 10 min before the test, with cannulae connected to Hamilton syringes through polyethylene tubing and mounted in an infusion pump. A subset of mice (n = 8) was coinjected with 0.5% Alexa Fluor 555–conjugated dextranamine (Invitrogen) to verify drug diffusion. The mouse was unrestrained and conscious during infusion (0.5 µl per side, 0.2 µl/min), which was allowed to diffuse for two additional minutes before reinserting dummy cannulae and returning to the home cage.

Tissue processing and staining

Mice were deeply anesthetized and transcardially perfused with ice-cold saline, followed by 4% formaldehyde in 0.1 M phosphate buffer (PB). Na_3VO_4 (1 mM) and NaF (50 mM) were added to saline and formaldehyde solutions when pErk1/2 immunostaining was planned. Brains were postfixed overnight (ON) at 4°C and transferred to 30% sucrose solution in PB until they sunk. Brains were frozen in dry ice and sliced at 25-µm thickness in a cryostat. Serial sections were kept in cryoprotector solution at −20°C until use. In most instances, virally expressed fluorophores were visualized without immuno-amplification. Sections were permeabilized with 0.3% Triton X-100 or 0.1% Tween-20 in buffer solution and incubated free floating in antibodies with 10% serum and 2% bovine serum albumin ON at 4°C. Primary antibodies were mouse anti-GAD67 (1:500) and goat anti-ChAT (1:250) from Millipore; guinea pig anti-VGAT (vesicular GABA transporter) (1:250) and guinea pig anti-RFP (1:500) from Synaptic Systems; rabbit anti-pErk1/2 #9101 from Cell Signaling at 1:300 (for brightfield) or 1:10,000 (for tyramide amplification); rabbit anti-PV, anti-calbindin, and anti-calretinin (all at 1:5000 from Swant); rabbit anti-somatostatin, anti–cholecystokinin-8, and anti-vasointestinal peptide (all at 1:2000 from Immunostar); goat or rabbit anti-cFos (#sc-52 at 1:1000 from Santa Cruz Biotechnology); and rabbit anti-WFS1 (1:500) from Proteintech. The next day, the tissue was washed and incubated for 2 hours in species-specific secondary antibodies conjugated to Alexa Fluor 488/555/647 (1:500, Invitrogen) or biotin (1:250, Vectorlabs). Tissue with biotinylated antibodies was further incubated with horseradish peroxidase–conjugated streptavidin (1:250, PerkinElmer) and visualized either with DAB or fluorescein isothiocyanate–conjugated tyramide (PerkinElmer) following manual instructions.

Imaging and analysis

Surgery cases included in the formal analysis were individually verified for successful viral expression, drug infusion, and anatomical location. Images were acquired using a Leica SP5 confocal microscope or a Leica AF6000 microscope for low magnification or brightfield. For comparisons of behavioral effects, laser power, spectral range, pinhole aperture, detector gain, and offset were initially set to obtain pixel densities within a linear range and were then kept constant between experimental groups or brain regions. To estimate the fraction of cells colabeled for cFos, pErk, or a type-specific marker, Z-series stacks of 1024 × 1024 pixel images (average of four scans per plane) were typically obtained from at least two to three consecutive sections per mouse (125 µm apart) with a 40× objective, thus obtaining a mean value per subject. Colabeling in somata was assessed near the midplane of individual cells based on 4′,6-diamidino-2-phenylindole counterstaining. To estimate the fractional CA1 input among afferent regions, ~1000 to 2000 YFP+ cells per series of sections were recorded per mouse. The neurochemical profile of MS^{CA1} cells was estimated from 973 reporter (+) cells and nine mice. The fractions of Fos + MS^{CA1} cells were estimated from 921 YFP+ cells and 25 mice; the neurochemical profile of hippocampal interneurons postsynaptic to MS was estimated from 254 green fluorescent protein (GFP)–positive cells and 3 mice; the fractions of Fos + CA1 interneurons after MS^{GABA} inhibition were estimated from 690 GAD+ cells and 25 mice; 3364 pErk+ cells in dorsal CA1 were analyzed from 44 mice with MS perturbations.

For quantification of axonal projections, z-stacks were collapsed, background substracted, thresholded, minimally filtered, and axons automatically selected in ImageJ; the created selection was then overlapped over the original image using the region of interest function, and the integrated intensity within was measured in a 100 µm by 100 µm square in each of the examined regions. In all cases, image acquisition was done blind to treatment group, and sampled regions were determined on the basis of precise anatomical identification, tissue preservation, and/or presence of the cells to be interrogated; the channel reporting the dependent measure was then visualized and recorded.

Statistics

Prism 8.2 (GraphPad) was used for statistical analysis. Two-tailed, unpaired *t* tests were used when comparing two datasets. To analyze multiple groups or regions, one-way analysis of variance (ANOVA), two-way ANOVA with post hoc Tukey's tests, or repeated-measures ANOVA with post hoc Sidak's tests were used as appropriate. Sample sizes ($n > 6$) for 90% power and $\alpha = 0.05$ took into account the mean ± SD of freezing behavior previously observed in wild-type conditioned mice in our laboratory (65 ± 16%, $n = 27$). A behaviorally relevant magnitude of difference was set to >30% based on previously published pharmacological effects on retrieval (*8*). Behavioral effects were validated through complementary approaches and further correlated with corresponding molecular effects, arguing against potential type I errors. Datasets were large enough to confirm with Shapiro-Wilk test and quantile-quantile plots that they followed a normal distribution. Error bars represent means ± SE. All *n* values represent individual mice.

SUPPLEMENTARY MATERIALS

Supplementary material for this article is available at http://advances.sciencemag.org/cgi/content/full/6/44/eaba5003/DC1

View/request a protocol for this paper from *Bio-protocol*.

REFERENCES AND NOTES

1. A. Ben-Yakov, Y. Dudai, M. R. Mayford, Memory retrieval in mice and men. *Cold Spring Harb. Perspect. Biol.* **7**, a021790 (2015).
2. D. S. Roy, A. Arons, T. I. Mitchell, M. Pignatelli, T. J. Ryan, S. Tonegawa, Memory retrieval by activating engram cells in mouse models of early Alzheimer's disease. *Nature* **531**, 508–512 (2016).
3. R. A. Cooper, F. R. Richter, P. M. Bays, K. C. Plaisted-Grant, S. Baron-Cohen, J. S. Simons, Reduced hippocampal functional connectivity during episodic memory retrieval in autism. *Cereb. Cortex* **27**, 888–902 (2017).
4. K. Z. Tanaka, A. Pevzner, A. B. Hamidi, Y. Nakazawa, J. Graham, B. J. Wiltgen, Cortical representations are reinstated by the hippocampus during memory retrieval. *Neuron* **84**, 347–354 (2014).
5. G. Vetere, J. W. Kenney, L. M. Tran, F. Xia, P. E. Steadman, J. Parkinson, S. A. Josselyn, P. W. Frankland, Chemogenetic interrogation of a brain-wide fear memory network in mice. *Neuron* **94**, 363–374 (2017).
6. I. Goshen, M. Brodsky, R. Prakash, J. Wallace, V. Gradinaru, C. Ramakrishnan, K. Deisseroth, Dynamics of retrieval strategies for remote memories. *Cell* **147**, 678–689 (2011).
7. K. Z. Tanaka, H. He, A. Tomar, K. Niisato, A. J. Y. Huang, T. J. McHugh, The hippocampal engram maps experience but not place. *Science* **361**, 392–397 (2018).
8. C. Zamorano, J. Fernández-Albert, D. R. Storm, X. Carné, C. Sindreu, Memory retrieval re-activates Erk1/2 signaling in the same set of CA1 neurons recruited during conditioning. *Neuroscience* **370**, 101–111 (2018).
9. M. A. Kheirbek, L. J. Drew, N. S. Burghardt, D. O. Costantini, L. Tannenholz, S. E. Ahmari, H. Zeng, A. A. Fenton, R. Hen, Differential control of learning and anxiety along the dorsoventral axis of the dentate gyrus. *Neuron* **77**, 955–968 (2013).
10. T. Kitamura, C. Sun, J. Martin, L. J. Kitch, M. J. Schnitzer, S. Tonegawa, Entorhinal cortical ocean cells encode specific contexts and drive context-specific fear memory. *Neuron* **87**, 1317–1331 (2015).
11. J.-H. Choi, S.-E. Sim, J.-i. Kim, D. I. Choi, J. Oh, S. Ye, J. Lee, T. H. Kim, H.-G. Ko, C.-S. Lim, B.-K. Kaang, Interregional synaptic maps among engram cells underlie memory formation. *Science* **360**, 430–435 (2018).
12. D. S. Roy, T. Kitamura, T. Okuyama, S. K. Ogawa, C. Sun, Y. Obata, A. Yoshiki, S. Tonegawa, Distinct neural circuits for the formation and retrieval of episodic memories. *Cell* **170**, 1000–1012.e19 (2017).
13. K. K. Cowansage, T. Shuman, B. C. Dillingham, A. Chang, P. Golshani, M. Mayford, Direct reactivation of a coherent neocortical memory of context. *Neuron* **84**, 432–441 (2014).
14. G. Unal, A. Joshi, T. J. Viney, V. Kis, P. Somogyi, Synaptic targets of medial septal projections in the hippocampus and extrahippocampal cortices of the mouse. *J. Neurosci.* **35**, 15812–15826 (2015).
15. T. F. Freund, M. Antal, GABA-containing neurons in the septum control inhibitory interneurons in the hippocampus. *Nature* **336**, 170–173 (1988).
16. P. Kaifosh, M. Lovett-Barron, G. F. Turi, T. R. Reardon, A. Losonczy, Septo-hippocampal GABAergic signaling across multiple modalities in awake mice. *Nat. Neurosci.* **16**, 1182–1184 (2013).
17. S. E. Rubio, G. Vega-Flores, A. Martínez, C. Bosch, A. Pérez-Mediavilla, J. del Río, A. Gruart, J. M. Delgado-García, E. Soriano, M. Pascual, Accelerated aging of the GABAergic septohippocampal pathway and decreased hippocampal rhythms in a mouse model of Alzheimer's disease. *FASEB J.* **26**, 4458–4467 (2012).
18. K. Tóth, T. F. Freund, R. Miles, Disinhibition of rat hippocampal pyramidal cells by GABAergic afferents from the septum. *J. Physiol.* **500**, 463–474 (1997).
19. R. Boyce, S. D. Glasgow, S. Williams, A. Adamantidis, Causal evidence for the role of REM sleep theta rhythm in contextual memory consolidation. *Science* **352**, 812–816 (2016).
20. T. Butler, K. Blackmon, L. Zaborszky, X. Wang, J. DuBois, C. Carlson, W. B. Barr, J. French, O. Devinsky, R. Kuzniecky, E. Halgren, T. Thesen, Volume of the human septal forebrain region is a predictor of source memory accuracy. *J. Int. Neuropsychol. Soc.* **18**, 157–161 (2012).
21. M. E. Hasselmo, What is the function of hippocampal theta rhythm?—Linking behavioral data to phasic properties of field potential and unit recording data. *Hippocampus* **15**, 936–949 (2005).
22. R. G. Phillips, J. E. LeDoux, Differential contribution of amygdala and hippocampus to cued and contextual fear conditioning. *Behav. Neurosci.* **106**, 274–285 (1992).
23. X. Chen, M. G. Garelick, H. Wang, V. Li, J. Athos, D. R. Storm, PI3 kinase signaling is required for retrieval and extinction of contextual memory. *Nat. Neurosci.* **8**, 925–931 (2005).
24. B. Zingg, X.-L. Chou, Z.-G. Zhang, L. Mesik, F. Liang, H. W. Tao, L. I. Zhang, AAV-mediated anterograde transsynaptic tagging: Mapping corticocollicular input-defined neural pathways for defense behaviors. *Neuron* **93**, 33–47 (2017).
25. F. Yi, J. Ball, K. E. Stoll, V. C. Satpute, S. M. Mitchell, J. L. Pauli, B. B. Holloway, A. D. Johnston, N. M. Nathanson, K. Deisseroth, D. J. Gerber, S. Tonegawa, J. J. Lawrence, Direct excitation of parvalbumin-positive interneurons by M_1 muscarinic acetylcholine receptors: Roles in cellular excitability, inhibitory transmission and cognition. *J. Physiol.* **592**, 3463–3494 (2014).
26. M. Jendryka, M. Palchaudhuri, D. Ursu, B. van der Veen, B. Liss, D. Kätzel, W. Nissen, A. Pekcec, Pharmacokinetic and pharmacodynamic actions of clozapine-N-oxide, clozapine, and compound 21 in DREADD-based chemogenetics in mice. *Sci. Rep.* **9**, 4522 (2019).
27. S. A. Thomas, Neuromodulatory signaling in hippocampus-dependent memory retrieval. *Hippocampus* **25**, 415–431 (2015).
28. F. Fuhrmann, D. Justus, L. Sosulina, H. Kaneko, T. Beutel, D. Friedrichs, S. Schoch, M. K. Schwarz, M. Fuhrmann, S. Remy, Locomotion, theta oscillations, and the speed-correlated firing of hippocampal neurons are controlled by a medial septal glutamatergic circuit. *Neuron* **86**, 1253–1264 (2015).
29. C. A. Campos, A. J. Bowen, C. W. Roman, R. D. Palmiter, Encoding of danger by parabrachial CGRP neurons. *Nature* **555**, 617–622 (2018).
30. A. I. Gulyás, M. Megías, Z. Emri, T. F. Freund, Total number and ratio of excitatory and inhibitory synapses converging onto single interneurons of different types in the CA1 area of the rat hippocampus. *J. Neurosci.* **22**, 10082–10097 (1999).
31. M. E. Hasselmo, C. Bodelón, B. P. Wyble, A proposed function for hippocampal theta rhythm: Separate phases of encoding and retrieval enhance reversal of prior learning. *Neural Comput.* **14**, 793–817 (2002).
32. J. Courtin, F. Chaudun, R. R. Rozeske, N. Karalis, C. Gonzalez-Campo, H. Wurtz, A. Abdi, J. Baufreton, T. C. M. Bienvenu, C. Herry, Prefrontal parvalbumin interneurons shape neuronal activity to drive fear expression. *Nature* **505**, 92–96 (2014).
33. J. Basu, J. D. Zaremba, S. K. Cheung, F. L. Hitti, B. V. Zemelman, A. Losonczy, S. A. Siegelbaum, Gating of hippocampal activity, plasticity, and memory by entorhinal cortex long-range inhibition. *Science* **351**, aaa5694 (2016).
34. A. Szőnyi, K. E. Sos, R. Nyilas, D. Schlingloff, A. Domonkos, V. T. Takács, B. Pósfai, P. Hegedüs, J. B. Priestley, A. L. Gundlach, A. I. Gulyás, V. Varga, A. Losonczy, T. F. Freund, G. Nyiri, Brainstem nucleus incertus controls contextual memory formation. *Science* **364**, eaaw0445 (2019).
35. L. A. DeNardo, C. D. Liu, W. E. Allen, E. L. Adams, D. Friedmann, L. Fu, C. J. Guenthner, M. Tessier-Lavigne, L. Luo, Temporal evolution of cortical ensembles promoting remote memory retrieval. *Nat. Neurosci.* **22**, 460–469 (2019).
36. F. Donato, S. B. Rompani, P. Caroni, Parvalbumin-expressing basket-cell network plasticity induced by experience regulates adult learning. *Nature* **504**, 272–276 (2013).
37. J. Haam, J. Zhou, G. Cui, J. L. Yakel, Septal cholinergic neurons gate hippocampal output to entorhinal cortex via oriens lacunosum moleculare interneurons. *Proc. Natl. Acad. Sci. U.S.A.* **115**, E1886–E1895 (2018).
38. G.-W. Zhang, L. Shen, W. Zhong, Y. Xiong, L. I. Zhang, H. W. Tao, Transforming sensory cues into aversive emotion via septal-habenular pathway. *Neuron* **99**, 1016–1028.e5 (2018).
39. E. Nanou, A. Lee, W. A. Catterall, Control of excitation/inhibition balance in a hippocampal circuit by calcium sensor protein regulation of presynaptic calcium channels. *J. Neurosci.* **18**, 4430–4440 (2018).

40. F. Xia, B. A. Richards, M. M. Tran, S. A. Josselyn, K. Takehara-Nishiuchi, P. W. Frankland, Parvalbumin-positive interneurons mediate neocortical-hippocampal interactions that are necessary for memory consolidation. *eLife* **6**, e27868 (2017).

Acknowledgments: We thank S. Sternson, L. Zhang, B. Roth, and K. Deisseroth for depositing plasmids to Addgene, and J. de la Rocha for support. **Funding:** This work was funded by grants SAF2012-40102, SAF2015-69767P (MINECO/FEDER), and Marie Curie CIG-631035 to C.S. **Author contributions:** A.S.-D., A.R., S.D., and C.S. performed and analyzed the experiments. H.M. provided reagents and supervised electrophysiology experiments. M.P. provided reagents and contributed to the experimental design. C.S. conceived and coordinated the project and wrote the manuscript. All authors contributed interpretation of the data and commented on the manuscript. **Competing interests:** The authors declare that they have no competing interests. **Data and materials availability:** All data needed to evaluate the conclusions in the paper are present in the paper and/or the Supplementary Materials. Additional data related to this paper may be requested from the authors.

Submitted 9 December 2019
Accepted 11 September 2020
Published 30 October 2020
10.1126/sciadv.aba5003

Citation: A. Sans-Dublanc, A. Razzauti, S. Desikan, M. Pascual, H. Monyer, C. Sindreu, Septal GABAergic inputs to CA1 govern contextual memory retrieval. *Sci. Adv.* **6**, eaba5003 (2020).

Science Advances

Septal GABAergic inputs to CA1 govern contextual memory retrieval

Arnau Sans-Dublanc, Adrià Razzauti, Srinidhi Desikan, Marta Pascual, Hannah Monyer and Carlos Sindreu

Sci Adv **6** (44), eaba5003.
DOI: 10.1126/sciadv.aba5003